



FPGA based modified multi-repeat distribution matcher for probabilistic amplitude shaping

Coincidencia de distribución de repetición múltiple modificada basada en FPGA para la conformación probabilística de amplitud

Ali Shaban Hassooni^{1,2*}, Laith Ali Abdul Rahaim¹

¹ Department of Electrical Engineering, college of Engineering, University of Babylon in Hilla, Iraq

² Department of Biomedical Engineering, college of Engineering, University of Babylon in Hilla, Iraq.

* eng.ali.shaban@uobabylon.edu.iq

(recibido/received: 29-mayo-2023; aceptado/accepted: 05-agosto-2022)

ABSTRACT

The technique of probabilistic amplitude modulation, based on distribution matching, has garnered considerable attention in recent years as a means to enhance spectral efficiency and diminish the constellation energy of coded modulation. This paper introduces the implementation of Probabilistic Amplitude Modulation (PAS) using a Modified Multi-Repeat Distribution Matcher (MMRDM) on a Field Programmable Gate Array (FPGA). The Modified Multiple Repetition Distribution Matcher (MMRDM) is integrated into a 2×2 Multiple Input Multiple Output Orthogonal Frequency Division Multiplexing (MIMO-OFDM) system, realized through the Xilinx System Generator (XSG). Simple Zero-Forced and Minimum Mean Squared Error (MMSE) equalizers are applied to the receiver for signal detection across the MIMO channel. The system incorporates enhanced security through chaos-based scrambling with 16 and 64 Quadrature Amplitude Modulation (QAM). VHDL code files for this system are generated for the Xilinx Kintex-7 (xc7k325t-3fbg676) for hardware implementation. Performance evaluation includes an assessment of required storage capacity, complexity, and bit error rate (BER). Using Vivado 2017.4, the system is successfully routed with resource utilization, for example, 0.67% Block RAM (BRAM), 68.6% Look-Up Tables (LUT), 83% DSP 48s, and 1.5% registers for 64-QAM uniform modulation. Similarly, for 64-QAM 10 level (shaper output 60 bit) shaped modulation, the resource utilization is 0.67% BRAM, 68.8% LUT, 83% DSP 48s, and 1.6% registers on the specified device. Simulation results demonstrate an improvement in the net shaping gain of approximately (2-4 dB) at 1×10^{-4} for different equalizer cases compared to uniform QAM, along with a notable reduction in required storage capacity and computational complexity.

Keywords: FPGA, MMRDM, MIMO, ZERO-FORCED, MMSE, Xilinx System Generator.

RESUMEN

La técnica de modulación de amplitud probabilística, basada en la adaptación de la distribución, ha atraído considerable atención en los últimos años como medio para mejorar la eficiencia espectral y disminuir la energía de la constelación de la modulación codificada. Este artículo presenta la implementación de la modulación de amplitud probabilística (PAS) utilizando un comparador de distribución de repetición múltiple modificado (MMRDM) en una matriz de puertas programables en campo (FPGA). El comparador de distribución de repetición múltiple modificado (MMRDM) está integrado en un sistema de multiplexación por división de frecuencia ortogonal de entrada múltiple y salida múltiple (MIMO-OFDM)

2×2, realizado a través del generador de sistema Xilinx (XSG). Se aplican ecualizadores simples de error cuadrático medio (MMSE) de fuerza cero simple y mínimo al receptor para la detección de señales a través del canal MIMO. El sistema incorpora seguridad mejorada mediante codificación basada en el caos con modulación de amplitud en cuadratura (QAM) de 16 y 64. Los archivos de código VHDL para este sistema se generan para Xilinx Kintex-7 (xc7k325t-3fbg676) para la implementación de hardware. La evaluación del rendimiento incluye una evaluación de la capacidad de almacenamiento requerida, la complejidad y la tasa de error de bits (BER). Con Vivado 2017.4, el sistema se enruta exitosamente con utilización de recursos, por ejemplo, 0,67 % de RAM de bloque (BRAM), 68,6 % de tablas de búsqueda (LUT), 83 % de DSP 48 y 1,5 % de registros para modulación uniforme de 64 QAM. De manera similar, para la modulación con forma de 64-QAM de 10 niveles (salida del moldeador de 60 bits), la utilización de recursos es 0,67 % de BRAM, 68,8 % de LUT, 83 % de DSP 48 y 1,6 % de registros en el dispositivo especificado. Los resultados de la simulación demuestran una mejora en la ganancia de conformación neta de aproximadamente (2-4 dB) a 1×10^{-4} para diferentes casos de ecualizador en comparación con QAM uniforme, junto con una reducción notable en la capacidad de almacenamiento requerida y la complejidad computacional.

Palabras claves: FPGA, MMRDM, MIMO, ZERO-FORCED, MMSE, Generador de sistemas Xilinx.

1. INTRODUCTION

Probabilistic shaping (PS) has emerged as a potent tool in digital signal processing (DSP) for various communication systems, particularly in achieving capacity-approaching performance and adapting rates in accordance with the Shannon limit (Böcherer et al., 2015; Buchali et al., 2015). In typical PS systems, distribution matching (DM) is positioned outside forward error correction (FEC) coding for simplified implementation. The utilization of digital subcarriers enables water filling performance (Che & Shieh, 2018) and mitigates the impact of equalizer-enhanced phase noise (Sun et al., 2020).

Several researchers (Bobrov & Dordzhiev, 2023; Civelli & Secondini, 2020; Guiomar et al., 2020; Gültekin et al., 2019) have proposed diverse transmission systems based on probabilistic shaping, resulting in enhanced system performance and confirming the efficacy of probabilistic shaping technology across different communication systems. Probabilistic amplitude shaping (PAS) coding modulation, proposed as an integration strategy between modulation and channel coding (Böcherer et al., 2015), has garnered considerable interest in both wireless and optical communications. The architecture of probabilistic amplitude shaping involves CCDM (Constant Composition Distribution Matching), utilizing arithmetic coding as a shaping algorithm, with performance improvements observed for longer data packets (Schulte & Böcherer, 2015). However, this integration, while showcasing excellent performance at quasi-infinite DM word lengths, poses high complexity for hardware implementation due to the use of arithmetic coding, despite simplification from outer concatenation.

Various DM algorithms, such as enumerative sphere shaping (ESS) (Gültekin et al., 2018), multiset-partition DM (Fehenberger et al., 2018), and DM with shell mapping (Schulte & Steiner, 2019), have been explored. Look-up table (LUT) based DMs have been applied in fixed-length hierarchical DM (Yoshida, Karlsson, et al., 2019a), fixed-length optimum bit-level DM with binomial coefficients (Koganei et al., 2019), and variable-length prefix-free code DM (J. Cho & Winzer, 2019). In cases of limited source entropy live traffic, joint source-channel coding has been shown to simultaneously compress data and shape to reduce average symbol energy based on sorting of LUT contents in the DM with minimal added complexity (Yoshida, Karlsson, et al., 2019b). (İşcan et al., 2019) utilized probabilistic shaping to enhance system performance in the 5G new radio system by introducing a polar encoder after the shaping encoder, resulting in over 1dB improvements on AWGN channels without increased computing requirements. Probabilistic amplitude shaping can be effectively implemented on a Field Programmable Gate Array (FPGA), offering versatility in integration into an Orthogonal Frequency Division Multiplexing-Multiple Input Multiple

Output (OFDM-MIMO) system. FPGAs are widely adopted in communication systems for their enhanced processing speed, parallelism in implementation, and cost reduction (Ganesh et al., 2015). Spatial multiplexing MIMO-OFDM implementation using FPGA has become a key area of interest for researchers (Chen et al., 2007; Kerttula et al., 2007; Mahendra Babu et al., 2014; Park & Ogunfunmi, 2012; Yoshizawa & Miyanaga, 2012), with various designs showcasing advancements in different aspects of communication systems. This paper proposes a modified method based on the multi-repeat distribution matcher principle (MRDM) (Jing et al., 2021; Yoshida et al., 2021; Yoshida, Binkai, et al., 2019) as a probabilistic shaping coder. The proposed method employs smaller lookup tables to create a coding scheme, significantly reducing required storage capacity without complex calculations, making it easily implementable on FPGA. The non-uniform distribution, akin to the MB distribution, is achieved by selecting the number of levels or subsets and symbols for repetition in each level, creating small lookup tables with the same number of levels according to the shaping rate required for shaping encoder and decoder formation. Altering the distribution enhances energy and spectrum efficiency, as the average symbol energy required to transmit data with a non-uniform distribution is lower than that of the same data transmitted with a uniform distribution at the same noise level. Mathematical analysis of bit error rate via AWGN and Massive-MIMO channels was performed, and simulations of MMRDM were conducted through a 2x2-MIMO OFDM channel with two different equalizers using the Xilinx System Generator. Results indicate significant improvements in storage capacity, computational complexities, and bit error rate (BER) when utilizing MMRDM compared to uniform QAM under the same channel and signal-to-noise ratio conditions.

2. SYSTEM MODEL

As illustrated in Figure 1, this paper employs a 2x2-MIMO OFDM communication system utilizing coded modulation based on rectangular QAM and MMRDM probabilistic shaping. On the transmitting end, the PAS encoder transforms the uniformly distributed bit stream into the desired distribution, which will be discussed in detail in the subsequent section. Following this, the conv-FEC encoder processes the shaped bits, and QAM mappers then associate these bits with QAM symbols. The 1x2 Serial2Parallel block is followed by two IFFT blocks. The signals are then transmitted through a 2x2 MIMO channel, represented by a blue diamond with four paths labeled h_{11} , h_{12} , h_{21} , and h_{22} .

Upon reaching the receiver and traversing the 2x2-MIMO channel, two types of equalizers (Zero-Forced and MMSE) are employed to reconstruct the original signal. The QAM demapper untangles the received signals by calculating Record Likelihood Ratios (LLRs) based on the observed signals. Subsequently, the FEC decoder receives the LLRs from the demapper to correct channel errors and maps them back to data bits through the shaping (invDM) decoder.

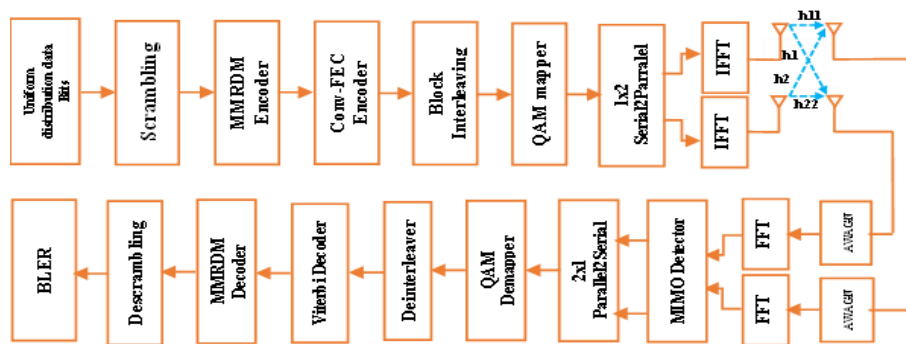


Figure 1. 2x2 MIMO-OFDM system

3. MODIFIED MULTI-REPEAT DISTRIBUTION MATCHER

As commonly understood, shaping coding operates on the principle of altering the distribution of data with a rate R_b from uniform to non-uniform. The objective is to minimize the average energy of symbols in the constellation by repeating points closest to the center, with lower energy, more frequently than distant points with higher energy. This approach is employed to enhance the overall performance of the system (K. Cho & Yoon, 2002). To achieve optimal results, the probability of the constellation signal point $r \in \mathbb{R}$ must adhere to Eq. 1.

$$p(r) = A(\lambda)e^{-\lambda r^2} \quad r \in \mathbb{R} \quad (1)$$

Where λ is a parameter governing the relationship and trade-off between average energy and bit rate, and as mentioned earlier, this distribution is the Maxwell-Boltzmann (MB) distribution.

In this proposed approach, the probabilistic shaping process involves the addition of extra bits to achieve a one-to-one mapping method, resulting in reduced computational complexity for the system. The method utilizes multiple repetition mapping of combinations instead of sequence permutation to derive the mapping sequence in the Probabilistic Amplitude Shaping (PAS). This technique is referred to as multi-repeat shaping (MRS) (Jing et al., 2021). The modification presented in this paper involves populating multiple lookup tables with constellation points based on the target rate as subsets, aiming to achieve a distribution similar to the MB distribution. Figure 2 provides an illustrative depiction of this method.

To begin, we define the number of levels or groups as L , followed by sub-groups of assignment groups denoted as S_1, \dots, S_L . Symbols, representing the constellation's points, consist of a group of bits according to the order of the constellation. For each level or subset, lookup tables are established. The output from these tables signifies the probabilistic encoding of the original input information for a given packet length (Jing et al., 2021).

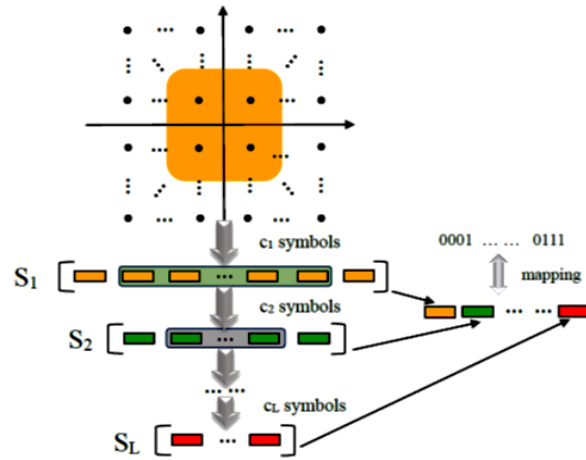


Figure 2. Shaping process.

It is crucial to carefully define the rules for selecting constellation symbols to ensure the flexibility of the shaping method. In the case of an M-QAM constellation, where there are M symbols, each symbol is composed of $N = \log_2(M)$ bits. Within each level, a certain number of these symbols will be repeated. For instance, in level S_1 , the number of symbols is denoted as c_1 . Subsequently, the S_2 subset is formed from S_1 , incorporating its symbols (c_2), and this process continues until reaching the final group S_L with its

designated number of symbols, c_L . The repetition of symbols follows the energy rule, meaning that symbols with lower energy undergo more repetition.

This approach achieves a one-to-one mapping of symbols across all subsets for a given block length of the original data. This mapping is designed to avoid the computational complexity associated with a many-to-one assignment resulting from a complex iterative method.

In this method, the main parameters that must be specified for the attainment of shaping encoding (Jing et al., 2021) are as follows:

- L: the number of levels
- N: the number of bits for each symbol within the M constellation
- c_1, c_2, \dots, c_L : the number of symbols in all the set groups
- m: the input information's block length

Parameters are related to each other based on these mathematical relationships:

$$\left\{ \begin{array}{l} c_1 \leq 2^N \\ c_2 \leq c_1 \\ \dots \dots \\ c_L \leq c_{L-1} \\ 2^m \leq c_1 \times c_2 \times \dots \times c_L \leq 2^{L \times N} \end{array} \right. \quad (2)$$

Let us suppose that the number set of vectors satisfied MB distribution PA' is $\zeta_{PA'}$

$$\zeta_{PA'} = c_1 \times c_2 \times \dots \times c_L \quad (3)$$

In that case, the input block length m will be as follows:

$$m = \lceil \log_2 c_1 \rceil + \dots + \lceil \log_2 c_L \rceil \quad (4)$$

The shaping rate R is.

$$R = m / (L \times N) \quad (5)$$

The codebook size of MRDM is $|C_{MRDM}| = 2^m$

The parameter L plays a crucial role in determining the trade-off between the divergence of the distribution from the MB distribution and the complexity of the shaping encoder. The maximum number of combined codewords is governed by L, and each symbol comprises N bits. Consequently, the storage capacity needed for the generated lookup table is calculated as $2^m \times (L \times N)$ bits. This implies that an increase in the number of levels and the modulation order results in heightened computational complexity and a significant increase in storage capacity. For instance, in the scenario where $L = 2$ and the modulation is 16-QAM (meaning $N=4$) with levels $c_1=4$ and $c_2 = 8$, based on Eq. (4), the block length m is 5. Therefore, the size of the lookup table will be $(2^5 \times 8)$ bits.

This implies that the storage capacity required would be minimal, but there would be a greater distribution divergence. However, by setting $L = 3$ for the same modulation and selecting levels with $c_1 = 4$, $c_2 = 8$, and $c_3 = 16$, based on Eq. (4), the block length $m = 9$. Consequently, the lookup table would be $(2^9 \times 12)$ bits, indicating an increase in storage capacity and a decrease in distribution divergence. Nevertheless, as the modulation order rises, the necessary capacity will surge significantly. To illustrate, consider 64-QAM with ten different energy levels and 64 symbols, where $N = 6$. Assuming $L = 8$ and levels $c_1 = 4$, $c_2 = 4$, $c_3 = 8$, $c_4 = 8$, $c_5 = 16$, $c_6 = 32$, $c_7 = 32$, $c_8 = 64$ using Eq. (4), it results in $m=30$ and the size of the lookup table being $(2^{30} \times 48)$, which is impractical due to its complexity.

To address this, we propose a modification to make the lookup table practical and easy to calculate. The lookup table is divided into smaller tables, each containing symbols equal to the number of symbols in each group. Returning to the previous examples, when $L = 2$, the size of the lookup table is 256 bits (Jing et al., 2021) Table I. With the modification, two lookup tables are created: the first containing 4 symbols, each represented by 4 bits, and the second containing 8 symbols represented by 4 bits. This reduces the storage requirement to only 3 bits for encoding tables, without the need for any table during the decoding process, as depicted in Figure 3. At $L=3$, the lookup table requires 6144 bits to store, but only 3 bits are needed when using multiple lookup tables for coding, as illustrated in Figure 4. For $L=8$ and 64-QAM modulation, the single lookup table needed would be $(2^{30} \times 48)$, which is impractical. However, with our modification, only 18 bits are required for the shaping and de-shaping process, as shown in Figure 5.

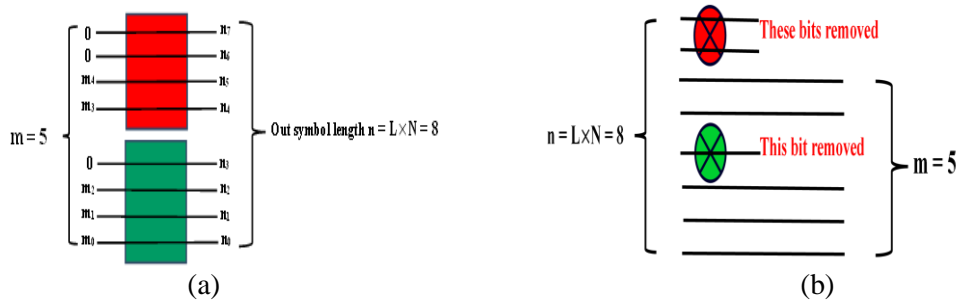


Figure 3. Shaping process for 16-QAM, $L=2$, $m=5$, $c_1=4$, $c_2=8$, and $N=4$ a) encoding b) decoding.

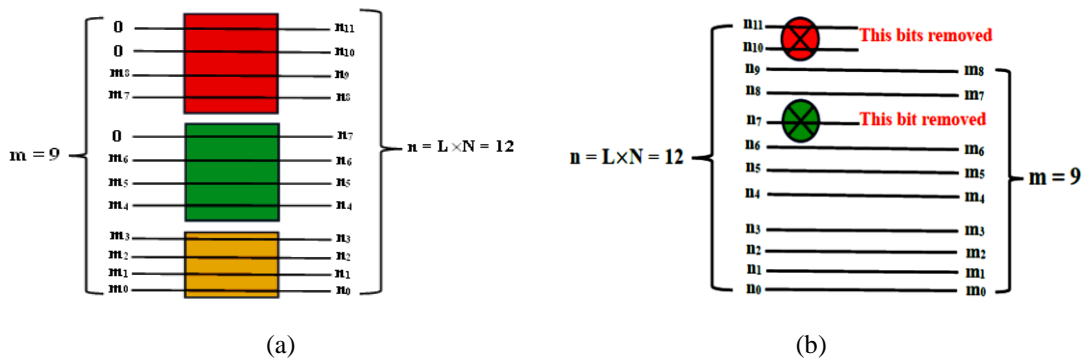


Figure 4. Shaping process for 16-QAM, $L=3$, $m=9$, $c_1=4$, $c_2=8$, $c_3=16$, and $N=4$ a) encoding b) decoding.

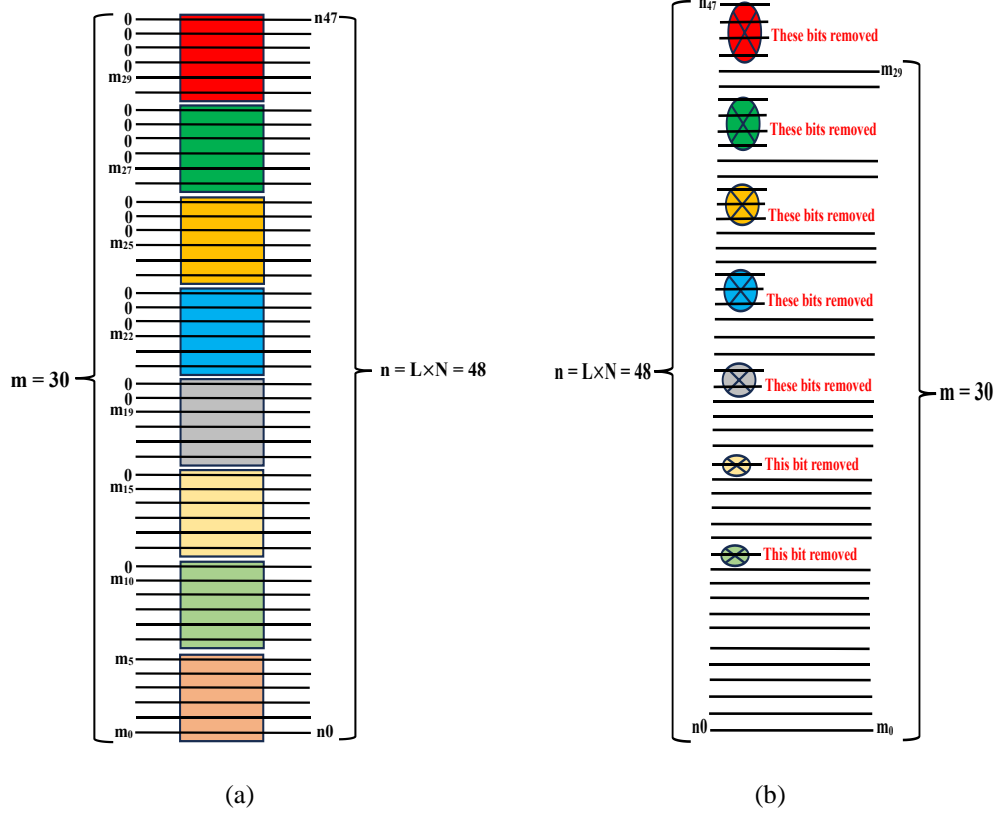


Figure 5. Shaping process for 64-QAM, $L=8$, $m=30$, $c_1 = 4$, $c_2 = 4$, $c_3 = 8$, $c_4 = 8$, $c_5 = 16$, $c_6 = 32$, $c_7 = 32$, $c_8 = 64$, and $N=6$ a) encoding b) decoding.

Eventually, from the MMRDM the probabilities of the generated distribution can be deduced as follows: QAM symbols probabilities are denoted by $p_A(a^M) = [p_{a1}, p_{a2}, \dots, p_{aM}]$, with L groups having varying probabilities.

group $g1$ comprises c_1 symbols with equal probabilities:

$$p_{g1}(a^{c1}) = \left[\frac{\frac{1}{c_1} + \frac{1}{c_2} + \dots + \frac{1}{c_L}}{L}, \dots, \frac{\frac{1}{c_1} + \frac{1}{c_2} + \dots + \frac{1}{c_L}}{L} \right]$$

group $g2$ comprises $(c_2 - c_1)$ symbols with equal probabilities.

$$p_{g2}(a^{c2}) = \left[\frac{\frac{1}{c_2} + \dots + \frac{1}{c_L}}{L}, \dots, \frac{\frac{1}{c_2} + \dots + \frac{1}{c_L}}{L} \right]$$

.

group gL comprises $(c_L - c_{L-1})$ symbols with equal probabilities.

$$p_{gL}(a^{cL}) = \left[\frac{1}{c_L}, \dots, \frac{1}{c_L} \right]$$

Subsequently, the PS-QAM probabilities are:

$$p_A(a^M) = p_{g1} \cup p_{g2} \cup \dots \cup p_{gL}.$$

4. MMRDM PERFORMANCE

As it is known that the QAM symbol error rate P_s through the AWGN channel can be expressed as (K. Cho & Yoon, 2002):

$$P_s = 4 \frac{\sqrt{M}-1}{\sqrt{M}} Q \left(\frac{d(M, E_b)}{\sqrt{2N_0}} \right) - 4 \left(\frac{\sqrt{M}-1}{\sqrt{M}} \right)^2 Q^2 \left(\frac{d(M, E_b)}{\sqrt{2N_0}} \right) \quad (6)$$

Parameter $d(M, E_b)$ denotes the minimum distance between constellation symbols. It is predicated on the number of symbols M , on the bit energy E_b as well as up to $N = \log_2 M$ the number of bits for each symbol. The symbols locations are $(\pm A, \pm 3A, \dots, \pm(\sqrt{M}-1)A) + i(\pm A, \pm 3A, \dots, \pm(\sqrt{M}-1)A)$ for the square QAM constellation, for QAM average symbols energy $E_{SQAM} = \frac{2}{3}(M-1)A^2$, and also for MMRDM QAM average symbols energy $E_{SMRDM} = \sum_{i=1}^M p_{AMRDM}(a_i) E(a_i)$. Thus, $E_{SMRDM} < E_{SQAM}$ and the value of $d_{min} = 2A$, which is why $A_{QAM} = \sqrt{3E_{SQAM}/2(M-1)}$, the expression of d_{min} is

$$d_{min_{QAM}} = 2 \sqrt{3E_{SQAM}/2(M-1)} = \sqrt{6E_{SQAM}/(M-1)} \quad (7)$$

And $d_{min_{MMRDM}} > d_{min_{QAM}}$

Apply these rules in 16-QAM as a case in point.

$$E_{SQAM} = 10A^2$$

$$d_{min_{QAM}} = \sqrt{2E_{SQAM}/5} \quad \text{sub. In Eq. (6)}$$

$$QAM \text{ symbol error rate } P_{s_{QAM}} = 3Q \left(\sqrt{\frac{E_{SQAM}}{5N_0}} \right) - \frac{9}{4} Q^2 \left(\sqrt{\frac{E_{SQAM}}{5N_0}} \right)$$

Since $E_s = \log_2(M) \times E_b$

$$P_{s_{QAM}} = 3Q \left(\sqrt{\frac{4E_b}{5N_0}} \right) - \frac{9}{4} Q^2 \left(\sqrt{\frac{4E_b}{5N_0}} \right) \quad (8)$$

$$QAM \text{ Bit error rate } P_{b_{QAM}} = \frac{P_{s_{QAM}}}{\log_2 M}$$

For 16-QAM with MMRDM, $L=2$

$$E_{SMRDM} = 4A^2, \text{ then the amplitude } A_{MMRDM} = \sqrt{E_{SMRDM}/4}$$

$$d_{min_{MMRDM}} = \sqrt{E_{SMRDM}} \quad \text{sub. In Eq. (6)}$$

$$P_{s_{MMRDM}} = 3Q \left(\sqrt{\frac{2E_b}{N_0}} \right) - \frac{9}{4} Q^2 \left(\sqrt{\frac{2E_b}{N_0}} \right) \quad (9)$$

$$\text{Bit error rate } P_{b_{MMRDM}} = \frac{P_{s_{MMRDM}}}{\log_2 M}$$

Upon comparing equations 8 and 9, it becomes evident that the symbol error rate in MMRDM QAM surpasses that in standard QAM. This improvement is attributed to the shaping process, wherein the symbol energy rate for the constellation decreases, resulting in an increased minimum distance (d_{min}) between the symbols compared to uniform QAM (Yu et al., 2020).

The performance of the proposed method can be assessed by calculating the achievable shaping gain ratio GMMRDM. This ratio is defined as the ratio between the shaping gain provided by PS-MMRDM using a QAM lattice of MMRDM size and the gain provided by the uniform QAM constellation of MQAM size, expressed as follows:

$$G_{MMRDM} = \frac{Y_{s_{MMRDM}}}{Y_{s_{QAM}}} = \frac{E_{QAM}}{E_{MMRDM}}$$

$$G_{MMRDM} \text{ dB} = 10 \log_{10} \left(\frac{\frac{1}{M_{QAM}} \sum_i^{M_{QAM}} |x_i|^2}{\sum_j^{M_{MMRDM}} |a_j|^2 p_{AMRDM}(a_j)} \right) \quad (10)$$

The gain ratio is determined to be 3.9dB by substituting the given values for $E_{QAM} = 10A^2$ and $E_{MMRDM} = 4A^2$.

To compute the storage capacity required for the proposed method, two scenarios are considered. First, if the selected subsets are powers of 2, the storage complexity is $(L \times \log_2 M - m)$. However, if any subset

ci is not a power of 2, then the storage capacity of the lookup table becomes $((L \times \log_2 M - m) + (k_1 2^{k_2} + k_3))$, where $k_1 = k_2 = \lfloor \log_2 ci \rfloor - 1$ and $k_3 = \log_2 M - (\lfloor \log_2 ci \rfloor + 2)$.

For ESS, the storage required depends on the number of energy levels L that satisfy the shaping rate Rs, which can be relatively large. The storage capacity required is expressed as (Gültekin et al., 2018) $L(N + 1)\lceil NR_s \rceil$ bits.

Next is the calculation of computational complexity, representing the arithmetic operations needed for encoding and decoding in the shaping methods. For the proposed method, two cases are considered. In the first case, if the levels or subgroups are powers of 2, no calculation process is needed for the sender or receiver, as depicted in Figures 3 and 4. However, if the level is not a power of 2, simple operations are required to find the address of the symbol in the lookup table, whether for the transmitter or the receiver. The time complexity for this subset is O(1). As for ESS, the number of bits operations required will be $(|\mathcal{A}_m - 1|)\lceil NR_s \rceil$ per symbol, whether for the transmitter or the receiver, where $|\mathcal{A}_m|$ represents the cardinality.

In conclusion, if subgroups are selected in the proposed method as powers of 2, the storage and computational complexity will be significantly lower compared to ESS. For instance, if the number of output symbols is 30, the modulation scheme used is 64-QAM, and $m = 120$, then the memory required for MMRSM is 60 bits only.

5. XILINX SYSTEM GENERATOR IMPLEMENTATION OF A MIMO-OFDM

Figure 6 illustrates the block diagram of the implemented key functions on the FPGA (Xilinx® kintex®-7 xc7k325t-3fbg676). Each block is constructed using Xilinx system generator (XSG) tools with a master clock period of 5 ns. The parameters employed for the MIMO-OFDM system are summarized in Table 1.

On the transmitter side, the random bit generator, operating at a rate of 200 Mbps, undergoes scrambling using a chaos-based stream ciphering method. The Multiple Repeat Distribution Matcher (MMRDM) alters the data distribution by introducing additional bits to the original bit, enabling the use of multiple lookup tables. MMRDM rates depend on the number of levels and the cardinality of each level according to equation 5. For instance, the rate of a 2-level MMRDM with 16-QAM is 5/8, and for a 3-level MMRDM, it is 3/4, as per equation 6. Figures 7 and 8 depict the XSG block diagram of 2 and 3 levels MMRDM encoders and decoders. The Convolution encoder encodes the binary scrambled stream bits with a code rate of 1/2, resulting in an output rate double that of the MMRDM rate. A matrix interleaver is then applied to produce interleaved stream bits. QAM modulation is utilized, generating complex modulated signals with a symbol rate equal to the Convolution encoder divide by N (symbol bits). The signal is then converted from serial to 2 parallel samples to achieve a rate twice that of the QAM symbol rate. Subsequently, the signal passes through the Inverse Fast Fourier Transform (IFFT) block to produce the OFDM signal, with the cyclic prefix guard omitted. One signal is transmitted through one antenna, and the other through the second antenna, effectively doubling the system's capacity. Following this, the signals are corrupted by a MIMO channel with flat fading and AWGN channels. On the receiving side, linear MMSE MIMO detection is employed to recover the clean signals. It is assumed that the channel estimation is perfect, and the channel parameters are directly inputted into the MMSE MIMO detection. All operations performed on the transmitted side are reversed on the receiving side to reconstruct the binary stream bits.

Table 1. MIMO-OFDM System Parameters

Clock	Antenna configuration	Modulation	Number of subcarrier	Coding	Coding rate	MIMO processing	MIMO Signaling
200MHz	2×2	16/64 QAM	16	Convolutional coding	1/2	MMSE	Spatial Multiplexing

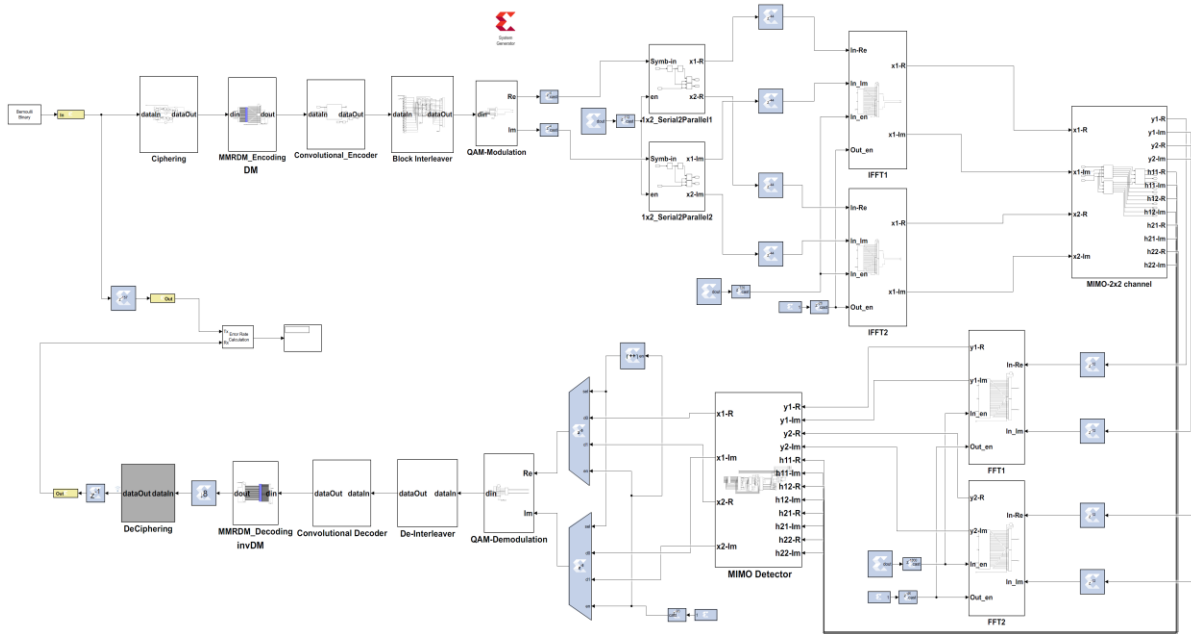


Figure 6. XSG block diagram of MIMO-OFDM transceiver.

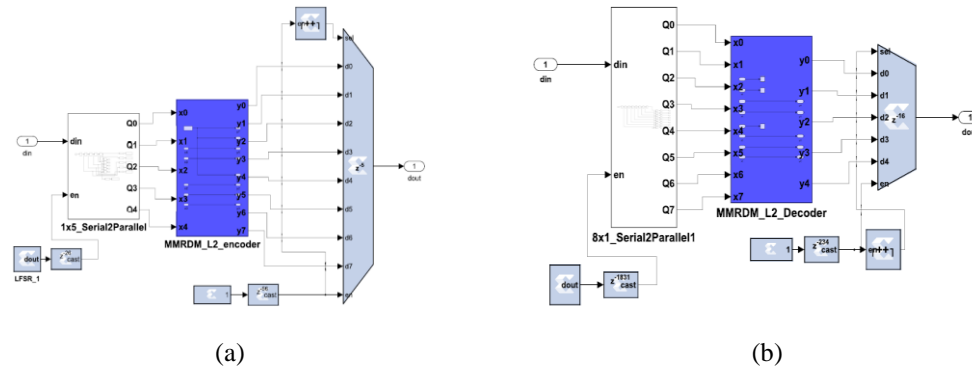


Figure 7. XSG block diagram of shaping process for 16-QAM, $L=2$, $m=5$, $c_1=4$, $c_2=8$, and $N=4$ a) encoding b) decoding.

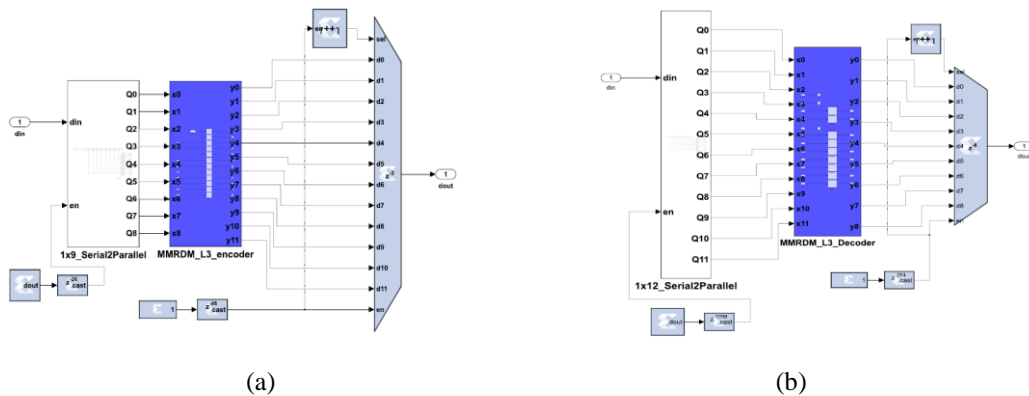


Figure 8. XSG block diagram of the shaping process for 64-QAM, $L=3$, $m=9$, $c_1=4$, $c_2=8$, $c_3=16$, and $N=4$ a) encoding b) decoding.

Returning to the probabilistic shape encoder, the method's efficiency has been theoretically demonstrated in terms of the required storage capacity and computational complexity. This efficiency will be further validated when implemented in the OFDM-MIMO system on an FPGA. For instance, when generating a VHDL Code or Bitstream file for various systems, the resources needed for uniform 16-QAM modulation are 0.67% BRAM, 67.12% LUT, 80.95% DSP 48s numbers, and 1.48% registers. In comparison, the required resources for L2-MMRDM 16-QAM are 0.67% BRAM, 67.15% LUT, 80.95% DSP 48s numbers, and 1.5% registers. The selected device shows only a marginal increase of 0.037% in LUT and 0.02% in registers over the uniform 16-QAM resources, with no increase in DSP 48s numbers, as demonstrated in Table 2. This table reveals the resource utilization on (Xilinx® kintex®-7 xc7k325t-3fbg676). It is evident that the MMRDM technique consumes minimal resources, and both the MMRDM encoder and decoder require no BRAM or DSP slices.

Table 2 Resources utilization

System	BRAM (445 available)	DSP 48s (840 available)	LUT (203800 available)	Registers (407600 available)
Uniform 16-QAM	3	680	136794	6058
MMRDM-L2	3	680	136869	6157
MMRDM-L3	3	680	136890	6169
Uniform 64-QAM	3	696	139904	6113
MMRDM-L8	3	696	140131	6420
MMRDM-L10	3	696	140147	6430

6. RESULTS AND DISCUSSION

In the proposed system, the base station employs OFDM-MIMO and is implemented using XSG in R2022b MATLAB software. System performance is assessed by focusing on parameters such as bit error rate (BER) and modulation gain ratio, crucial for evaluating communication system reliability. In the simulation of the MMRDM-OFDM-MIMO system, a data block size ranging between 2, 246, 4000 and 2, 995, 2000 bits is selected. Figures 9 depict the BER as a function of signal-to-noise ratio (SNR) for 16QAM and 64QAM, considering a 2x2 MIMO system with both transmitting and receiving antennas.

In Figure 9(a), where the number of MMRDM groups is $L=2$ and $L=3$, the performance is compared to uniform 16-QAM. In Figure 9(b), the number of shaping groups is $L=8$ and $L=10$, and they are compared to uniform 64-QAM, specifically for the Zero-Forced type equalizer. Noticeable improvements in BER are observed with MMRDM compared to uniform QAM, showing an improvement of about (2-4) dB at 10^{-4} BER. Figure 10 introduces the MMSE equalizer for the same probabilistic shaping combinations and FEC rate, demonstrating that MMRDM probabilistic modulation consistently provides better performance than uniform QAM in both systems, with an improvement of about 2-2.5 dB at 10^{-4} BER.

As evident in Figures 9 and 10, the number of levels (L) plays a crucial role in balancing the deviation of the input data distribution from the MB distribution, the encryption formation rate, and the associated complexities in terms of computational demands and required storage capacity. With an increase in L , the rate rises, and rate losses decrease, while the required storage capacity increases but remains low in MMRDM, as highlighted in Table 2.

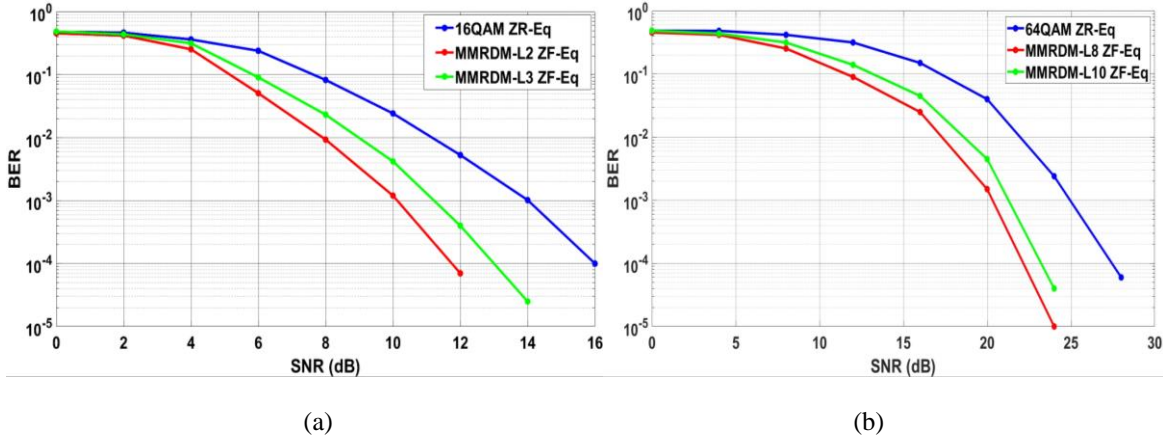


Figure 9. Performance of ZERO-FORCED MIMO-OFDM system over flat fading channel (a) 16QAM (b) 64QAM.

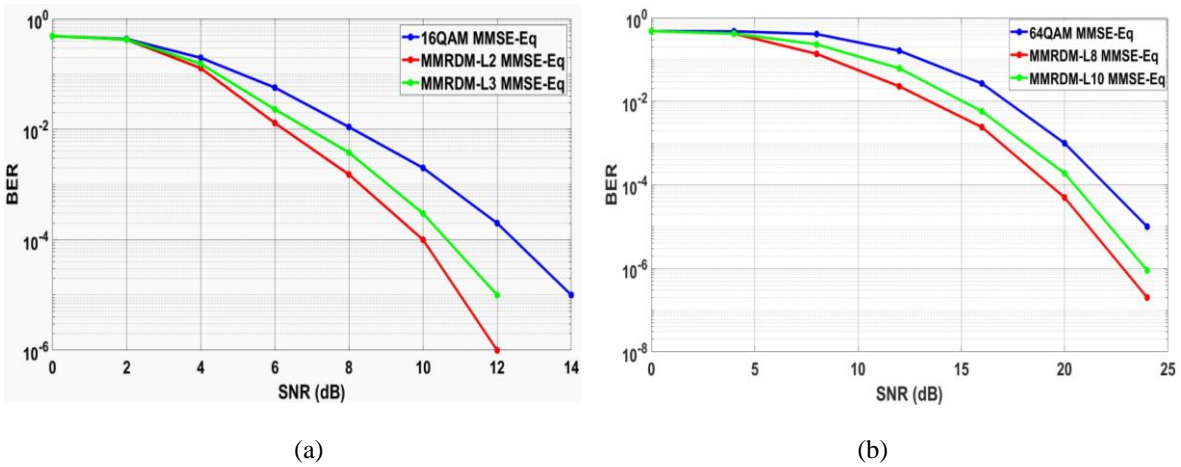


Figure 10. Performance of MMSE MIMO-OFDM system over flat fading channel (a) 16QAM (b) 64QAM.

7. CONCLUSIONS

This study explores the application of the MMRDM-based probabilistic shaping technique in a 2×2 MMSE MIMO-OFDM communication system implemented on an FPGA using the Xilinx system generator. Our findings demonstrate enhancements in system performance, simplification of the shaping process without imposing computational complexity or extensive storage requirements. Notably, the memory demand is minimal compared to the data block length. Furthermore, the application of Eq. (10), representing the shaping gain ratio, leads to substantial improvements in energy efficiency, coupled with a noteworthy reduction in Bit Error Rate (BER). Both results and mathematical analyses underscore the favorable shaping advantages conferred by the MMRDM method.

In the FPGA implementation, it is noteworthy that, as detailed in Table 2, the MMRDM encoder and decoder exhibit efficiency, requiring neither (BRAM) nor DSP slices, and demonstrating low utilization of Look-Up Tables (LUT) and registers.

REFERENCIAS

Bobrov, E., & Dordzhiev, A. (2023). On Probabilistic QAM Shaping for 5G MIMO Wireless Channel with Realistic LDPC Codes. *ArXiv Preprint ArXiv:2303.02598*.

- Böcherer, G., Steiner, F., & Schulte, P. (2015). Bandwidth efficient and rate-matched low-density parity-check coded modulation. *IEEE Transactions on Communications*, 63(12), 4651–4665.
- Buchali, F., Steiner, F., Böcherer, G., Schmalen, L., Schulte, P., & Idler, W. (2015). Rate adaptation and reach increase by probabilistically shaped 64-QAM: An experimental demonstration. *Journal of Lightwave Technology*, 34(7), 1599–1609.
- Che, D., & Shieh, W. (2018). Approaching the capacity of colored-SNR optical channels by multicarrier entropy loading. *Journal of Lightwave Technology*, 36(1), 68–78.
- Chen, J., Zhu, W., Daneshrad, B., Bhatia, J., Kim, H.-S., Mohammed, K., Sasi, S., & Shah, A. (2007). A real time 4×4 MIMO-OFDM SDR for wireless networking research. *2007 15th European Signal Processing Conference*, 1151–1155.
- Cho, J., & Winzer, P. J. (2019). Multi-rate prefix-free code distribution matching. *2019 Optical Fiber Communications Conference and Exhibition (OFC)*, 1–3.
- Cho, K., & Yoon, D. (2002). On the general BER expression of one-and two-dimensional amplitude modulations. *IEEE Transactions on Communications*, 50(7), 1074–1080.
- Civelli, S., & Secondini, M. (2020). Hierarchical distribution matching for probabilistic amplitude shaping. *Entropy*, 22(9), 958.
- Fehenberger, T., Millar, D. S., Koike-Akino, T., Kojima, K., & Parsons, K. (2018). Multiset-partition distribution matching. *IEEE Transactions on Communications*, 67(3), 1885–1893.
- Ganesh, G. V, Krishna, B. M., Kumar, K. S., Prathyusha, T., Venkatesh, R., & Jessy, T. V. (2015). FPGA implementation of OFDM transmitter using Simulink and Xilinx system generator. *Journal of Theoretical and Applied Information Technology*, 78(1), 125.
- Guiomar, F. P., Lorences-Riesgo, A., Ranzal, D., Rocco, F., Sousa, A. N., Fernandes, M. A., Brandão, B. T., Carena, A., Teixeira, A. L., & Medeiros, M. C. R. (2020). Adaptive probabilistic shaped modulation for high-capacity free-space optical links. *Journal of Lightwave Technology*, 38(23), 6529–6541.
- Gültekin, Y. C., van Houtum, W. J., Koppelaar, A. G. C., Willems, F. M. J., & Wim, J. (2019). Enumerative sphere shaping for wireless communications with short packets. *IEEE Transactions on Wireless Communications*, 19(2), 1098–1112.
- Gültekin, Y. C., Willems, F. M. J., Van Houtum, W. J., & Şerbetli, S. (2018). Approximate enumerative sphere shaping. *2018 IEEE International Symposium on Information Theory (ISIT)*, 676–680.
- İşcan, O., Böhnke, R., & Xu, W. (2019). Probabilistic shaping using 5G new radio polar codes. *IEEE Access*, 7, 22579–22587.
- Jing, Z., Tian, Q., Xin, X., Ding, J., Yu, J., Pan, X., Zhang, Q., Zhu, L., Tian, F., & Wang, Y. (2021). A multi-repeat mapping based probabilistic shaping coding method applied to data center optical networks. *Optical Fiber Technology*, 61, 102401.
- Kerttula, J., Myllylä, M., & Juntti, M. (2007). Implementation of a K-best based MIMO-OFDM detector algorithm. *2007 15th European Signal Processing Conference*, 2149–2153.
- Koganei, Y., Sugitani, K., Nakashima, H., & Hoshida, T. (2019). Optimum bit-level distribution matching with at most $O(N^3)$ implementation complexity. *2019 Optical Fiber Communications Conference and Exhibition (OFC)*, 1–3.
- Mahendra Babu, D. S., Vinutha, M. R., & Uma, C. (2014). Design and Implementation of MIMO-OFDM using Encoding and Decoding techniques on FPGA. *International Journal of Scientific & Engineering Research*, 5(6), 939–

944.

Park, J. S., & Ogunfunmi, T. (2012). Efficient FPGA-based implementations of MIMO-OFDM physical layer. *Circuits, Systems, and Signal Processing*, 31, 1487–1511.

Schulte, P., & Böcherer, G. (2015). Constant composition distribution matching. *IEEE Transactions on Information Theory*, 62(1), 430–434.

Schulte, P., & Steiner, F. (2019). Divergence-optimal fixed-to-fixed length distribution matching with shell mapping. *IEEE Wireless Communications Letters*, 8(2), 620–623.

Sun, H., Torbatian, M., Karimi, M., Maher, R., Thomson, S., Tehrani, M., Gao, Y., Kumpera, A., Soliman, G., & Kakkar, A. (2020). 800G DSP ASIC design using probabilistic shaping and digital sub-carrier multiplexing. *Journal of Lightwave Technology*, 38(17), 4744–4756.

Yoshida, T., Binkai, M., Koshikawa, S., Chikamori, S., Matsuda, K., Suzuki, N., Karlsson, M., & Agrell, E. (2019). FPGA implementation of distribution matching and dematching. *45th European Conference on Optical Communication (ECOC 2019)*, 1–4.

Yoshida, T., Igarashi, K., Konishi, Y., Karlsson, M., & Agrell, E. (2021). FPGA Implementation of Hierarchical Subcarrier Rate and Distribution Matching for up to 1.032 Tb/s or 262144-QAM. *Optical Fiber Communication Conference, Tu6D-4*.

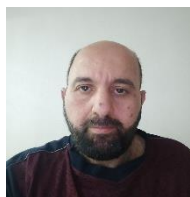
Yoshida, T., Karlsson, M., & Agrell, E. (2019a). Hierarchical distribution matching for probabilistically shaped coded modulation. *Journal of Lightwave Technology*, 37(6), 1579–1589.

Yoshida, T., Karlsson, M., & Agrell, E. (2019b). Joint source-channel coding via compressed distribution matching in fiber-optic communications. *2019 Optical Fiber Communications Conference and Exhibition (OFC)*, 1–3.

Yoshizawa, S., & Miyanaga, Y. (2012). Hardware Development of Baseband Transceiver and FPGA-Based Testbed in 88 and 22 MIMO-OFDM Systems. *ECTI Transactions on Computer and Information Technology (ECTI-CIT)*, 6(1), 64–71.

Yu, Q., Corteselli, S., & Cho, J. (2020). FPGA implementation of rate-adaptable prefix-free code distribution matching for probabilistic constellation shaping. *Journal of Lightwave Technology*, 39(4), 1072–1080.

SEMBLANZA DE LOS AUTORES



Ali Shaban Hassooni    is an Asst. Professor at the Department of Biomedical Engineering, University of Babylon, Iraq, was born in Babylon-1981, Iraq. He received the B.Sc. degree in Electrical engineering Department from the University of Babylon (2003)-Iraq, M.Sc. degrees in Electronics and Communication Engineering from the University of Babylon-Iraq in 2011. He is a Ph.D student in University of Babylon. Since 2006, he has been with the University of Babylon-Iraq, His research interests include Optimization, OFDM, MIMO-OFDM, CDMA, , Modulation Technique, Signal processing, Mathematical Modelling. He can be contacted at

email: eng.ali.shaban@uobabylon.edu.iq.



Laith Ali Abdul-Rahaim    is a Professor (Member IEEE) at the Department of Electrical Engineering, University of Babylon, Iraq, was born in Babylon-1972, Iraq. He received the B.Sc. degree in Electronics and Communications Department from the University of Baghdad (1995)-Iraq, M.Sc. and Ph.D. degrees in Electronics and Communication Engineering from the University of Technology-Iraq in 2001 and 2007 respectively. Since 2003, he has been with the University of Babylon-Iraq, His research interests include MC-CDMA, OFDM, MIMO-OFDM, CDMA, Space Time Coding, Modulation Technique, Image processing. He can be contacted at

email: drlaithanzy@uobabylon.edu.iq.